

# Laplacian Analysis Meets Dynamics Modelling: Gaussian Splatting for 4D Reconstruction

Yifan Zhou <sup>\*</sup> <sup>1</sup>, Beizhen Zhao <sup>\*</sup> <sup>1</sup>, Pengcheng Wu <sup>2</sup>, Hao Wang <sup>†</sup> <sup>1</sup>

<sup>1</sup> The Hong Kong University of Science and Technology (Guangzhou)

<sup>2</sup> Nanyang Technological University

yifanzhou@hkust-gz.edu.cn, bzha0610@connect.hkust-gz.edu.cn, pengchengwu@ntu.edu.sg, haowang@hkust-gz.edu.cn

## Abstract

While 3D Gaussian Splatting (3DGS) excels in static scene modeling, its extension to dynamic scenes introduces significant challenges. Existing dynamic 3DGS methods suffer from either over-smoothing due to low-rank decomposition or feature collision from high-dimensional grid sampling. This is because of the inherent spectral conflicts between preserving motion details and maintaining deformation consistency at different frequency. To address these challenges, we propose a novel dynamic 3DGS framework with hybrid explicit-implicit functions. Our approach contains three key innovations: a spectral-aware Laplacian encoding architecture which merges Hash encoding and Laplacian-based module for flexible frequency motion control, an enhanced Gaussian dynamics attribute that compensates for photometric distortions caused by geometric deformation, and an adaptive Gaussian split strategy guided by KDTree-based primitive control to efficiently query and optimize dynamic areas. Through extensive experiments, our method demonstrates state-of-the-art performance in reconstructing complex dynamic scenes, achieving better reconstruction fidelity.

## Introduction

Dynamic scene reconstruction from monocular videos presents a critical challenge in computer vision, demanding precise modeling of both persistent geometric structures and transient deformations (Cai et al. 2022; Du et al. 2021; Fang et al. 2022; Kratimenos, Lei, and Daniilidis 2024; Li, Slavcheva et al. 2022). Unlike static environments, dynamic scenes exhibit heterogeneous motion patterns - rigid components maintain temporal consistency while deformable regions require high-frequency trajectory modeling (Xu et al. 2024; Duan et al. 2024; Bae et al. 2024). This inherent complexity creates dual challenges: preserving spatial coherence across time-varying geometries and capturing transient deformation details without over-smoothing artifacts.

While Neural Radiance Fields (NeRF) (Mildenhall et al. 2021; Chan et al. 2022; Yang, Vo et al. 2022; Park et al. 2021b; Martin-Brualla et al. 2021) revolutionized static scene modeling through continuous volumetric integration, their dynamic extensions (Choe et al. 2023; Gao et al. 2021; Liang, Laidlaw et al. 2023; Liu et al. 2023; Wang et al. 2023;

Barron et al. 2021; Fridovich-Keil et al. 2023) reveal critical limitations in handling temporal discontinuities, particularly the conflicting requirements for spatial fidelity versus temporal coherence arising from uniform spectrum allocation. Although explicit representations (Barron, Mildenhall et al. 2023; Cao and Johnson 2023; Tancik et al. 2022) improve efficiency through 4D spacetime factorization, their low-rank decomposition induces feature collision in overlapping regions. Recent 3D Gaussian Splatting (3DGS) (Kerbl et al. 2023; Duisterhof et al. 2023; Yang et al. 2023; Liang et al. 2023; Lin et al. 2024) has achieved impressive effects for static environments, where discrete volumetric primitives enable both photorealistic rendering and computationally efficient optimization through differentiable rasterization (Shao et al. 2023; Wu et al. 2024; Lu et al. 2024; Luiten et al. 2024; Kratimenos, Lei, and Daniilidis 2024).

However, their direct extension to dynamic scenarios faces three fundamental limitations: 1) existing deformable methods suffer from either over-smoothing due to low-rank decomposition or feature collision from high-dimensional grid sampling, 2) previous Gaussian-based methods use a fixed threshold during Gaussian split stage which ignore adaptive split adjustment, and 3) persistent appearance changes caused by dynamic deformation are often neglected in current pipelines.

To address the challenges above, our key insight lies in addressing the anisotropic spatio-temporal sampling nature of dynamic scenes through hybrid explicit-implicit encoding. First, we develop a hybrid spectral-aware encoder combining Hash grids with Laplacian-based module that decouples spatial and temporal features into different frequency motion components, overcoming the feature collision of low-rank assumption while enabling adaptive frequency motion control. Then, we design an enhanced Gaussian dynamics attribute to perform individual Gaussian personalized dynamic optimization and design an adaptive regularization for identifying highly dynamic areas. Besides, we propose an adaptive Gaussian split strategy, which focuses on the optimization trade-off between Gaussian shape and anisotropy in dynamic scenes and an improved KDTree-based clustering algorithm was proposed to efficiently query and optimize dynamic Gaussians.

Our solution rethinks dynamic 3DGS through Laplacian spectral analysis, which provides a hybrid framework for

<sup>\*</sup>These authors contributed equally to this work.

<sup>†</sup>Corresponding author.

localized frequency analysis. Meanwhile, we focus on the dynamics attribute of each Gaussian and the optimization problem in the derivation process, and propose a novel hybrid explicit-implicit algorithm model. We propose three key innovations. In summary, our contributions are as follows:

- We propose a spectral-aware Laplacian encoding module combining multi-scale Hash encoding with Laplacian-based dynamic module that decouples different frequency motion trajectories from complex deformation.
- We design an enhanced Gaussian dynamics attribute that identify highly dynamic areas for adaptive split and regularization.
- We design an adaptive Gaussian split strategy that automatically adjusts the primitive density and anisotropy using KDTree-guided spectral analysis.

## Related Work

### NeRF-based Dynamic Modeling

The advent of Neural Radiance Fields (NeRF) has significantly transformed the landscape of 3D scene reconstruction, particularly for static environments. However, extending NeRF to effectively model dynamic scenes remains a formidable challenge. Initial efforts, such as D-NeRF (Pumarola et al. 2021) and Nerfies (Park et al. 2021a), have employed canonical space warping and temporal latent codes to capture motion. Despite their innovative approaches, these methods often exhibit limitations when dealing with rapid or abrupt movements. Moreover, explicit spacetime factorization techniques, such as HexPlane (Cao and Johnson 2023), have been proposed to enhance computational efficiency. However, these methods impose restrictive low-rank assumptions that may oversimplify the intricate dynamics present in real-world scenes, particularly in environments characterized by rapid changes. Furthermore, while segmenting scenes into components with distinct attributes has been explored to enhance modeling accuracy (Gao et al. 2021; Tretschk, Tewari et al. 2021), the implicit representations based on fully connected MLPs often suffer from over-smoothing and lengthy training processes.

### 3DGS-based Dynamic Modeling

Recent advances in 3D Gaussian Splatting (3DGS) (Kerbl et al. 2023; Yu et al. 2024; Huang et al. 2024; Li et al. 2024) have demonstrated remarkable success in static scene reconstruction, prompting extensions to dynamic scenarios. While 4D-GS (Wu et al. 2024) employs multi-resolution HexPlanes with MLPs for deformation modeling, it inherits the fundamental limitation of plane-based methods: the low-rank assumption leads to feature collisions and rendering artifacts in complex motions. Neural deformation fields (Yang et al. 2024; Huang et al. 2024) address this through MLPs, but often produce over-smoothed results and struggle with high-frequency details due to insufficient inductive biases. Direct optimization of 4D Gaussians (Yang et al. 2023; Duan et al. 2024) offers greater flexibility but introduces optimization challenges including floating artifacts and requires extensive training with additional regularizers. Grid4D (Xu

et al. 2024) has achieved impressive performance through combining triplane and Hash-coding while it often lacks smoothness and works without an explicit method for modeling dynamic processes. While SplineGS (Park et al. 2024) proposes a pipeline that combine 3DGS and spline functions, however, it requires massive priors such as 2D trajectory and depth estimation to maintain performance. These limitations collectively highlight the need for a representation that balances expressiveness with efficient optimization for dynamic 3DGS, particularly in handling complex motions while preserving fine details. Our work addresses these limitations through a novel Laplacian motion representation that jointly optimizes for physical plausibility, computational efficiency, and multi-scale temporal fidelity.

## Methodology

In this section, we present our methodology aimed at addressing the challenges of modeling 4D dynamic scenes with high-fidelity spatial details and complex temporal variations. The key innovation lies in a hybrid explicit-implicit representation that combines multi-scale Hash encoding with spectral decomposition to capture spatial features and adaptive temporal dynamics. This framework is structured into three main components: spectral-aware Laplacian encoding module, enhanced Gaussian dynamic attribute and adaptive Gaussian split strategy. This hybrid approach is designed to enhance the representation of motion dynamics while maintaining physical consistency across spatial and temporal domains, significantly outperforming existing methods in handling complex motion patterns. The overall pipeline is shown in Fig. 1.

### Spectral-Aware Laplacian Encoding Module

This section focuses on the challenge of effectively encoding spatial and temporal information to capture the dynamics of motion. We employ a spectral-aware Laplacian encoding module that decomposes the frequency motion trajectories to accommodate the complexities of 4D spacetime.

**Multi-Scale Hash Encoding** To efficiently encode 4D spacetime information while preserving both spatial and temporal details, we employ a multi-scale hash encoding strategy that extends traditional methods. Inspired by Grid4D (Xu et al. 2024), we extend InstantNGP’s Hash encoding (Müller et al. 2022) to 4D spacetime  $(x, y, z, t)$  through anisotropic multi-resolution decomposition.

$$\mathcal{H}^l = \{\mathcal{H}_{xyz}^l, \mathcal{H}_{xyt}^l, \mathcal{H}_{yzt}^l, \mathcal{H}_{xzt}^l\}, \quad l \in \{1, \dots, L\} \quad (1)$$

Each level  $l$  maintains dimension-specific resolutions computed via geometric progression.

**Laplacian-Based Motion Prediction** In the realm of dynamic scene reconstruction, accurately predicting motion dynamics is paramount. Traditional methods often rely on MLP or linear interpolation, which fails to capture the complex periodic and aperiodic motions present in real-world dynamic scenes. To overcome these limitations, we propose a novel hybrid explicit-implicit Laplacian-based mo-

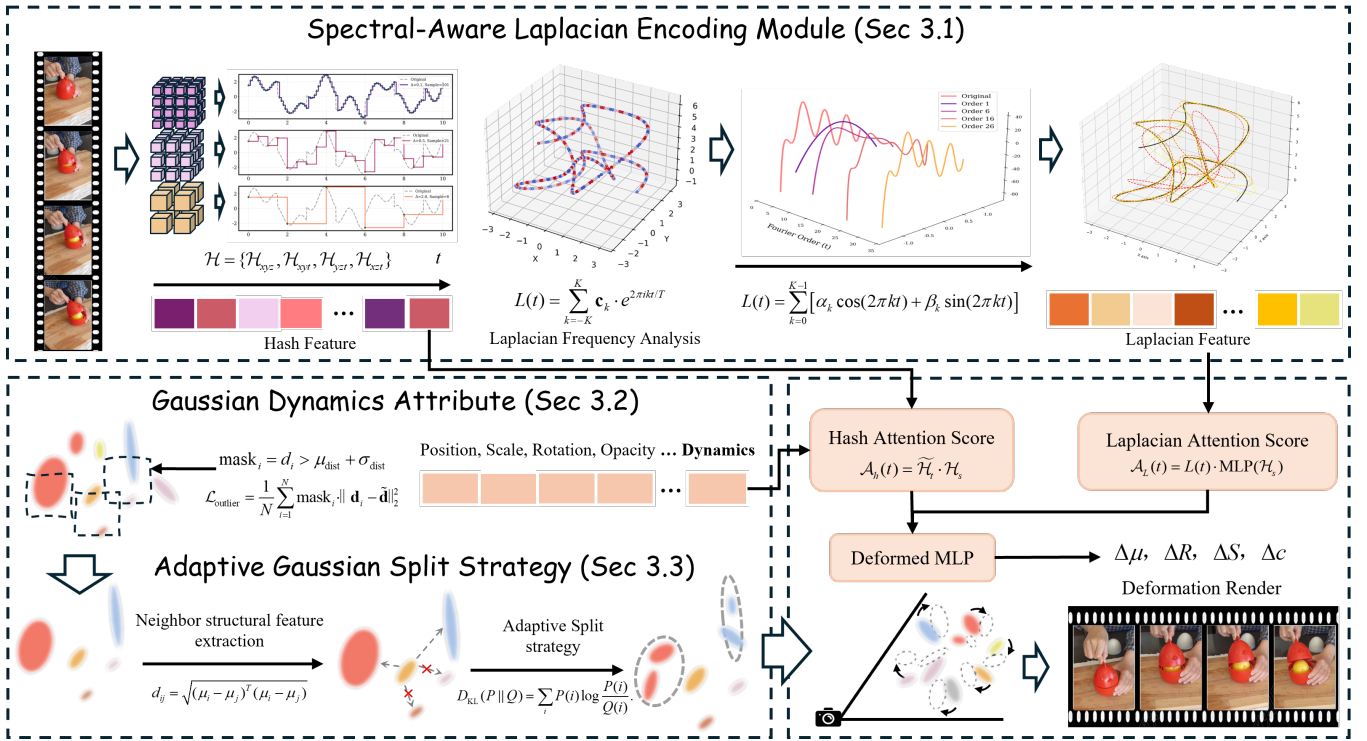


Figure 1: **Framework of our method.** We begin with a multi-scale Hash encoder to extract spatio-temporal features of Gaussians. Then a hybrid laplacian-based dynamic module is designed for adaptive frequency analysis. We design an appearance adjustment module which combines the Gaussian dynamic attribute with the spatio-temporal feature by attention mechanism. The whole pipeline benefits from the adaptive dynamic Gaussian split strategy for better performance and efficiency.

tion representation that combines the expressiveness of spectral analysis learnable neural components, allowing for the effective capture of both low and high-frequency motion dynamics. The foundation of our approach lies in the Laplacian series decomposition of time series:

$$L(t) = \sum_{k=-K}^K \mathbf{c}_k \cdot e^{2\pi i k t / T}, \quad (2)$$

where  $L(t)$  represents the Laplacian motion field at time  $t$ , with  $\mathbf{c}_k$  denoting coefficients. Through Euler's formula, we substitute this representation into our motion prediction:

$$L(t) = \sum_{k=-K}^K \mathbf{c}_k \cdot \cos\left(\frac{2\pi k t}{T}\right) + i \sum_{k=-K}^K \mathbf{c}_k \cdot \sin\left(\frac{2\pi k t}{T}\right). \quad (3)$$

This transformation naturally handles periodic motions common in dynamic scenes and the frequency components provide interpretable control over motion characteristics. To further enhance our motion representation, we extend the equation to a simple formulation:

$$L(t) = \sum_{k=0}^{K-1} [\alpha_k \cos(2\pi k t) + \beta_k \sin(2\pi k t)]. \quad (4)$$

Here, coefficients  $(\alpha_k, \beta_k)$  are learnable parameters. This design aims to automatically adapt to scene-specific motion frequencies while maintaining end-to-end differentiability. The Laplacian-based decoding allows our model to learn appropriate frequency compositions directly from data, eliminating the need for manual frequency band selection.

The orthogonal basis properties enable stable gradient computation during optimization. The incorporation of learnable frequencies  $f_k$  through gradient enhances the ability to capture different frequency motion components:

$$\frac{\partial \mathcal{L}}{\partial f_k} = \frac{1}{\sigma_k^2} \sum_t \left( \frac{\partial \mathcal{L}}{\partial L(t)} \cdot t \cdot [-\alpha_k \sin(2\pi f_k t) + \beta_k \cos(2\pi f_k t)] \right), \quad (5)$$

where  $\sigma_k$  denotes temporal variance. This mechanism automatically balances frequency preservation with motion stability. Then we introduce an attention mechanism which combines Laplacian features with Hash spatial features  $\mathcal{H}_s$ :

$$\mathcal{A}_L(t) = L(t) \cdot \text{MLP}(\mathcal{H}_s). \quad (6)$$

**Multi-Scale Laplacian Pyramid Supervision** To enforce consistency across different frequency bands and spatial scales, we introduce a multi-scale supervision strategy that enforces consistency across frequency bands, enhancing the model's ability to better detail preservation. We supervise reconstruction using Laplacian pyramid decomposition:

$$\mathcal{L}_{\text{lap}} = \sum_{l=1}^L \lambda_l \|\mathcal{L}_l(I_{\text{render}}) - \mathcal{L}_l(I_{\text{gt}})\|_1, \quad (7)$$

where  $\lambda_l$  decreasing exponentially to emphasize finer details. This loss function encourages the model to focus on both coarse and fine features, ensuring a comprehensive understanding of motion dynamics.

### Enhanced Gaussian Dynamics Attribute with Adaptive Regularization

To effectively model the dynamic variations inherent in complex scenes, we augment the standard 3D Gaussian Splatting representation. Specifically, we associate each 3D Gaussian  $G_i$  with a learnable dynamics attribute, denoted as  $\mathbf{d}_i \in \mathbb{R}^{D_d}$ , where  $D_d$  represents the dimensionality of this attribute space. The dynamics attribute  $\mathbf{d}_i$  is introduced to explicitly encapsulate these latent per-Gaussian temporal or conditional variations, providing a dedicated representation for dynamic properties.

To further improve the modeling of dynamic scene changes, we introduce a fusion mechanism that concatenates the original dynamic attribute vector  $\mathbf{d}_i$  with the Hash temporal feature  $\mathcal{H}_t$ , forming an augmented feature representation:

$$\tilde{\mathcal{H}}_t = \text{Concatenate}(\mathbf{d}_i, \mathcal{H}_t). \quad (8)$$

This concatenation provides a straightforward yet effective means of integrating scene-specific temporal information with the Gaussian’s intrinsic dynamic attributes, enabling the model to leverage both sources for more accurate deformation prediction. To effectively combine spatial and temporal information, we introduce an attention mechanism to aggregate spatio-temporal features through:

$$A_h(t) = \tilde{\mathcal{H}}_t \cdot \mathcal{H}_s. \quad (9)$$

**Adaptive Dynamic Regularization** To ensure that our method better model dynamic changes, we implement a selective regularization mechanism that targets only those Gaussians exhibiting ”abnormally large” or ”highly dynamic” changes. These Gaussians are referred to as ”outliers”, which need to be increase their gradients and thus promote their deformation or dynamic transformations.

Instead of using fixed thresholds or applying a regularization on all Gaussians, our method employs a data-driven, adaptive dynamic selection scheme. Specifically, for each Gaussian, we compute the Euclidean distance between its dynamic attribute  $\mathbf{d}_i$  and a reference mean dynamic attribute  $\bar{\mathbf{d}}$ , as well as the associated standard deviation:

$$d_i = \|\mathbf{d}_i - \bar{\mathbf{d}}\|_2. \quad (10)$$

Let  $\mu_{\text{dist}}$  and  $\sigma_{\text{dist}}$  denote the mean and standard deviation of all  $d_{\text{dist}_i}$  across the Gaussian set. We then generate a mask to identify those points that are significantly deviating from the typical embedding variation:

$$\text{mask}_i = d_i > \mu_{\text{dist}} + \sigma_{\text{dist}}. \quad (11)$$

Only the Gaussians satisfying this outlier criterion—i.e., those with  $\text{mask}_i = 1$ —are subjected to the additional regularization loss:

$$\mathcal{L}_{\text{dy}} = \frac{1}{N} \sum_{i=1}^N \text{mask}_i \cdot \|\mathbf{d}_i - \bar{\mathbf{d}}\|_2^2. \quad (12)$$

The purpose of this selective regularization is to intensify the gradients for Gaussians exhibiting large changes, thereby explicitly promoting their deformation and densification. By employing this dynamic regularization mechanism, the model adaptively concentrates regularization efforts on the most informative and dynamically relevant regions, effectively enhancing the capacity to model complex scene dynamics without imposing uniform constraints across all Gaussians.

In addition, we use Normalized cross-correlation (NCC) (Yoo and Han 2009) based loss function  $\mathcal{L}_{\text{NCC}}$  to evaluate the similarity between two images within local regions while maintaining invariance to brightness variations to enhance the alignment accuracy. The total loss  $\mathcal{L}$  used for training is composed of four distinct loss terms, each weighted by a corresponding hyperparameter  $\lambda$  to control its relative contribution. The total loss is formulated as:

$$\mathcal{L} = \mathcal{L}_{\text{orig}} + \lambda_{\text{NCC}} \mathcal{L}_{\text{NCC}} + \lambda_{\text{lap}} \mathcal{L}_{\text{lap}} + \lambda_{\text{dy}} \mathcal{L}_{\text{dy}}, \quad (13)$$

where  $\mathcal{L}_{\text{orig}}$  denotes original loss function of 3DGS and consists of  $\mathcal{L}_1$  and Structural Similarity Index Measure (SSIM) loss functions (Wang et al. 2004)  $\mathcal{L}_{\text{SSIM}}$ .

### Adaptive Gaussian Split Strategy

In this section, we address the challenge of optimizing Gaussian representations of motion dynamics. Our approach utilizes the analysis about the structure of each Gaussian to adaptively refine Gaussian parameters based on local neighborhood information, enhancing the model’s ability to capture complex motion patterns.

**KDTree-Based Primitive Analysis** To maintain spatial coherence and prevent overfitting, we analyze Gaussian primitives through their neighborhood relationships. For each Gaussian  $\mathcal{G}_i$ , we find  $K$  nearest neighbors  $\{\mathcal{G}_j\}_{j=1}^K$  based on Euclidean distance:

$$ed_{ij} = \sqrt{(\mu_i - \mu_j)^T (\mu_i - \mu_j)}. \quad (14)$$

By examining the size and anisotropy of each Gaussian (Xie, Zong et al. 2024), we can determine which Gaussians exhibit significant differences in their motion characteristics. Covariance differences are computed through L2 norm:

$$\Delta \Sigma_{ij} = \|\Sigma_i - \Sigma_j\|_2. \quad (15)$$

This adaptive approach ensures that our models remain responsive to local variations in motion dynamics. By focusing on Gaussians with notable differences in size and anisotropy, we can selectively choose which Gaussian to split, thereby enhancing the model’s ability to represent complex motion patterns without introducing unnecessary complexity.

**KL-Divergence Guided Adaptation** In some cases, we observed that the KDTree-based partitioning method can not accurately identify the dynamic Gaussian, which leads to the instability to capture dynamic motions. This is because the strategy of splitting Gaussian based on hard threshold will stop deriving when the shape and size of Gaussian in the neighborhood are similar. However, it is possible that some Gaussian in the neighborhood still contribute to the dynamic modeling. To further refine the Gaussian split process, we compute the KL-divergence between the neighbor Gaussian distribution  $P$  and a uniform distribution  $Q$ :

$$D_{\text{KL}}(P \parallel Q) = \sum_{k=1}^K P(k) \log \frac{P(k)}{Q(k)} \quad (16)$$

The adaptive splitting threshold  $\tau$  becomes:

$$\tau = \Delta\Sigma + D_{\text{KL}} \cdot \tau_{\text{base}} \quad (17)$$

where  $\tau_{\text{base}}$  is a hyperparameter. This mechanism allows for dynamic adjustments to the model’s complexity based on the observed motion patterns. Through adaptive dynamic Gaussian optimization strategy, we can determine when a Gaussian should be split more effectively, ensuring the model captures the nuances of motion dynamics while maintaining computational efficiency. This strategy enhances the model’s robustness against overfitting by focusing on the most relevant Gaussian structures.

## Experiment

### Experiment Setup

We evaluate our proposed method using three widely recognized datasets, comprising two real-world datasets and one synthetic dataset. The Neu3D (Li, Slavcheva et al. 2022) dataset is a real-world collection that features multiple static cameras and includes between 18 to 21 multi-view videos. We generate 300 frames for each video and initial point clouds for each scene following 4DGaussians (Wu et al. 2024). HyperNeRF (Park et al. 2021b) is a real-world dataset that captures continuous views with intricate topological variations at each timestamp within a dynamic scene. In our experiment, we utilized the “vrig” subset, which was captured using stereo cameras, training the model with data from one camera while validating it with data from the other. The D-NeRF (Pumarola et al. 2021) dataset serves as a synthetic dataset tailored for monocular scenes, with each scene comprising between 50 to 200 frames. Due to discrepancies between the training and testing scenarios presented in the Lego subset of the D-NeRF (Pumarola et al. 2021) dataset, we excluded it from our experimental analysis.

### Comparisons

On the Neu3D dataset, our approach demonstrates exceptional proficiency as shown in Tab. 3. The primary challenge here lies in accurately modeling intricate, often non-rigid, temporal dynamics while simultaneously reconstructing high-fidelity static scene geometry from these fixed perspectives. Our method excels in generating temporally coherent motion representations and preserving sharp geomet-

ric details throughout the sequences, effectively disentangling dynamic elements from the static background. In contrast, competing methods frequently struggle to maintain long-term temporal consistency across the multiple views, often exhibiting noticeable motion blur, particularly during complex actions or over extended durations.

The HyperNeRF “vrig” subset introduces a distinct set of demanding conditions. This dataset tests the model’s ability to handle complex motion while maintaining consistency across stereo viewpoints and adapt to evolving scene topology. Our method showcases remarkable resilience and adaptability in handling these extreme deformations and effectively leverages the stereo information, generalizing robustly across the viewpoints even when trained on one and validated on the other as shown in Tab. 1 and Fig. 3. It consistently reconstructs intricate topological changes with greater accuracy and fewer visual artifacts or geometric distortions compared to existing approaches.

Furthermore, evaluation on the synthetic D-NeRF dataset underscores our method’s inherent strength in inferring coherent 3D structure and plausible motion from limited input as shown in Tab. 2 and Fig. 2. Reconstructing dynamic 3D geometry from a single, potentially moving, camera viewpoint over time presents profound depth ambiguities and necessitates strong priors and temporal reasoning. Despite this inherent ill-posedness and the scarcity of explicit geometric cues, our approach generates remarkably temporally stable and geometrically plausible reconstructions. Consequently, it significantly outperforms baseline methods, which, under these monocular constraints, often exhibit pronounced depth inaccuracies that betray instabilities in their representation.

Across this diverse range of evaluated datasets, our method consistently achieves a marked superiority in performance. This advantage is evident in both the final reconstruction fidelity and the accurate, coherent capture of dynamic motion, ranging from subtle deformations to large-scale topological changes. This consistent success across varied and demanding conditions robustly validates the effectiveness, versatility, and broad applicability of our proposed framework for dynamic scene reconstruction.

### Ablation Study and Analysis

To validate the effectiveness of each component within our framework, we conduct comprehensive ablation studies to validate the necessity of each component as shown in Tab. 4, Tab. 5 and Fig. 4.

**Effect of Laplacian-Based Motion Prediction** Replacing this module with a defrom MLP leads to poorer performance, especially in scenes with diverse motion patterns or objects of varying sizes evolving over time. Dynamic scenes inherently possess variations across multiple spatial and temporal scales. This module is designed to capture these hierarchies effectively. It allows the model to represent fine details of motion trajectories while enabling the modeling of slow, gradual changes. By processing information hierarchically, it ensures consistent and accurate representation of scene dynamics across different frequency.

Table 1: **Quantitative comparison to previous methods on HyperNeRF (Park et al. 2021b) dataset.** The higher PSNR( $\uparrow$ ) and higher SSIM( $\uparrow$ ) denote better rendering quality. The color of each cell shows the **best** and the **second best**.

Scene Method	broom2			vrig-3dprinter			vrig-chicken			vrig-peel-banana			Aveage		
	SSIM $\uparrow$	PSNR $\uparrow$	LPIPS $\downarrow$	SSIM $\uparrow$	PSNR $\uparrow$	LPIPS $\downarrow$	SSIM $\uparrow$	PSNR $\uparrow$	LPIPS $\downarrow$	SSIM $\uparrow$	PSNR $\uparrow$	LPIPS $\downarrow$	SSIM $\uparrow$	PSNR $\uparrow$	LPIPS $\downarrow$
HyperNeRF (Park et al. 2021b)	0.210	19.51	—	0.635	20.04	—	0.828	27.46	—	0.719	22.15	—	0.598	22.29	—
D3DGS (Yang et al. 2024)	0.269	19.99	0.700	0.656	20.71	0.277	0.640	22.77	0.363	0.853	25.95	0.155	0.605	22.35	0.374
MotionGS (Zhu et al. 2024)	0.380	22.30	—	0.710	21.80	—	0.790	26.80	—	0.690	28.20	—	0.643	24.78	—
MoDec-GS (Kwak et al. 2025)	0.303	21.04	0.666	0.706	22.00	0.265	0.834	28.77	0.197	0.873	28.25	0.173	0.679	25.02	0.325
4DGaussians (Wu et al. 2024)	0.366	22.01	0.557	0.705	21.98	0.327	0.806	28.49	0.297	0.847	27.73	0.204	0.681	25.05	0.346
ED3DGS (Bae et al. 2024)	0.371	21.84	0.531	0.715	22.34	0.294	0.836	28.75	0.185	0.867	28.80	0.178	0.697	25.43	0.297
Grid4D (Xu et al. 2024)	0.414	21.78	0.423	0.723	22.36	0.245	0.848	29.27	0.199	0.875	28.44	0.167	0.715	25.46	0.259
Ours	0.422	22.36	0.413	0.724	22.56	0.264	0.858	29.57	0.166	0.876	28.81	0.169	0.720	25.83	0.253

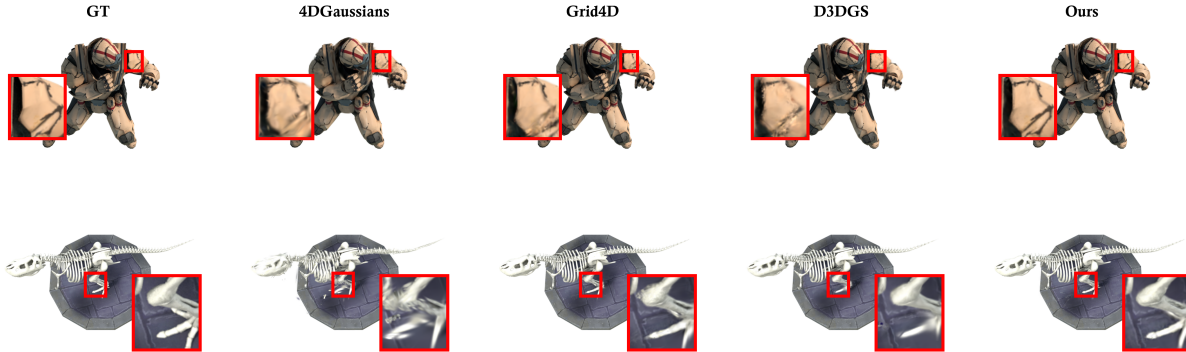


Figure 2: **Comparison Results.** Visual differences are highlighted with red insets for better clarity. Our approach consistently outperforms other models on D-NeRF (Pumarola et al. 2021) dataset, demonstrating clear advantages in challenging scenarios such as thin geometries and fine-scale details. Best viewed in color.

Table 2: **Quantitative comparison to previous methods on D-NeRF (Pumarola et al. 2021) dataset.** The color of each cell shows the **best** and the **second best**. More detail results can be found in supplementary material.

Method	SSIM $\uparrow$	PSNR $\uparrow$	LPIPS $\downarrow$
3DGS (Kerbl et al. 2023)	0.930	23.40	0.077
K-Planes (Fridovich-Keil et al. 2023)	0.970	31.41	0.047
HexPlane (Cao and Johnson 2023)	0.972	31.92	0.038
4DGaussians (Wu et al. 2024)	0.985	35.32	0.021
D3DGS (Yang et al. 2024)	0.991	40.08	0.013
SC-GS (Huang et al. 2024)	0.993	41.66	0.009
Grid4D (Xu et al. 2024)	0.994	41.99	0.008
Ours	0.994	42.17	0.007

**Effect of Adaptive Gaussian Split Strategy** Removing this component and reverting to original 3DGS split strategy results in a drop in reconstruction. Crucially, this component offers a dual benefit. Firstly, it enhances reconstruction quality by intelligently allocating Gaussian primitives. It adaptively densifies regions with high dynamics while pruning redundant or insignificant Gaussians. This leads to a more accurate representation of the scene and results in a more compact set of Gaussians compared to non-adaptive methods while achieving similar quality as shown in Tab. 4.

Table 3: **Quantitative comparison to previous methods on Neu3D (Li, Slavcheva et al. 2022) dataset.** Color of each cell shows the **best** and the **second best**. We show the average results of all scenes. More detail results can be found in supplementary material.

Method	SSIM $\uparrow$	PSNR $\uparrow$	LPIPS $\downarrow$
4DGaussians (Wu et al. 2024)	0.935	30.36	0.152
Grid4D (Xu et al. 2024)	0.934	30.50	0.147
Spacetime (Li et al. 2024)	0.944	31.46	0.142
ED3DGS (Bae et al. 2024)	0.943	31.92	0.139
Ours	0.944	32.12	0.134

**Effect of Laplacian Pyramid Loss** When this loss is removed on the rendered image, we observe a noticeable degradation in reconstruction quality. The Laplacian pyramid loss decomposes the reconstruction error across multiple frequency bands by comparing the Laplacian pyramids of the rendered and ground truth images. This loss function proves essential because it enforces structural consistency across different scales, effectively preserving fine details that would otherwise be lost in single-scale supervision.

**Effect of Gaussian dynamics attribute** Compared with our full approach, removing the Gaussian dynamics attribute leads to poorer performance. This performance difference

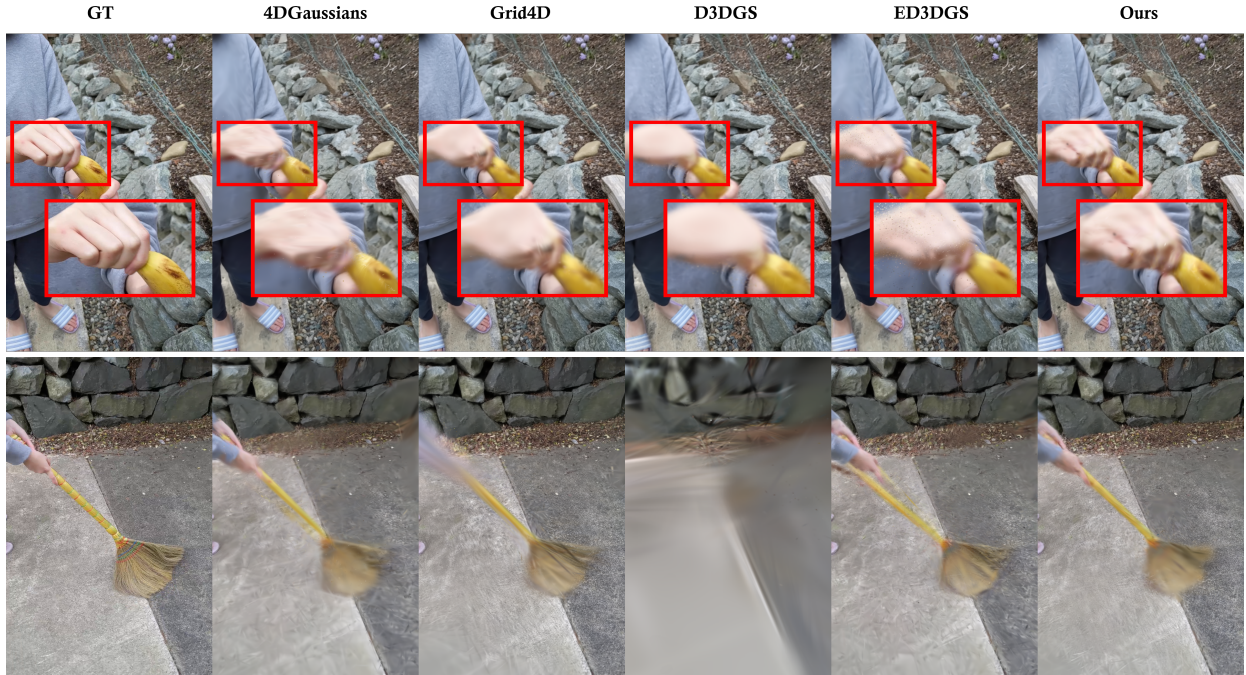


Figure 3: **Comparison Results.** Our approach consistently outperforms other models on HyperNeRF (Park et al. 2021b) dataset, demonstrating clear advantages in challenging scenarios. Best viewed in color.

Table 4: **Ablation Results on Neu3D (Li, Slavcheva et al. 2022) dataset.** The Adaptive Gaussian Split Strategy helps reduce the number of Gaussians.

Method	Gaussian Counts
w/o adaptive split strategy	589k
Ours	433k

Table 5: **Ablation evaluation on Neu3D (Li, Slavcheva et al. 2022) dataset.** The color of each cell shows the **best**.

Method	SSIM $\uparrow$	PSNR $\uparrow$	LPIPS $\downarrow$
w/o Laplacian module	0.938	31.64	0.149
w/o dynamic attribute	0.938	31.72	0.147
w/o adaptive split strategy	0.943	31.96	0.133
w/o $\mathcal{L}_{lap}$	0.939	31.70	0.148
Ours	0.944	32.12	0.134

underscores the importance of embedding dedicated dynamic attributes within the Gaussians themselves. By incorporating these dynamic attribute, our method allows each Gaussian to better adapt its shape and orientation according to its specific local dynamics, effectively capturing details and mitigating the feature collision issues inherent in relying solely on lower-rank spatio-temporal grids.



Figure 4: **Ablation Results.** Replacing Laplacian-based motion prediction leads to poorer performance.

## Conclusion

In this paper, we present a novel approach for dynamic 3DGS that addresses the challenges of anisotropic spatio-temporal sampling through a hybrid explicit-implicit encoding framework. We introduced three key innovations: Firstly, a hybrid motion representation combining multi-scale Hash encoding with a Laplacian-based dynamic module, effectively decoupling different motion frequencies from complex deformation details. Secondly, an enhanced Gaussian dynamics attribute that compensates for highly dynamic areas induced by geometric deformation. Thirdly, an adaptive Gaussian split strategy guided by KDTree-based analysis, which automatically adjusts dynamic primitive density and anisotropy. This work advance the state-of-the-art in dynamic scene modeling by bridging the gap between explicit representations and spectral analysis, with potential applications in VR/AR and scene reconstruction.

## References

- Bae, J.; Kim, S.; Yun, Y.; Lee, H.; Bang, G.; and Uh, Y. 2024. Per-gaussian embedding-based deformation for deformable 3d gaussian splatting. In *European Conference on Computer Vision*, 321–335. Springer.
- Barron, J. T.; Mildenhall, B.; Tancik, M.; Hedman, P.; Martin-Brualla, R.; and Srinivasan, P. P. 2021. Mip-nerf: A multiscale representation for anti-aliasing neural radiance fields. In *Proceedings of the IEEE/CVF international conference on computer vision*, 5855–5864.
- Barron, J. T.; Mildenhall, B.; et al. 2023. Zip-nerf: Anti-aliased grid-based neural radiance fields. In *Proceedings of the IEEE/CVF International Conference on Computer Vision*, 19697–19705.
- Cai, H.; Feng, W.; Feng, X.; Wang, Y.; and Zhang, J. 2022. Neural surface reconstruction of dynamic scenes with monocular rgb-d camera. *Advances in Neural Information Processing Systems*, 35: 967–981.
- Cao, A.; and Johnson, J. 2023. Hexplane: A fast representation for dynamic scenes. In *Proceedings of the IEEE/CVF Conference on Computer Vision and Pattern Recognition*, 130–141.
- Chan, E. R.; Lin, C. Z.; Chan, M. A.; Nagano, K.; Pan, B.; De Mello, S.; Gallo, O.; Guibas, L. J.; Tremblay, J.; Khamis, S.; et al. 2022. Efficient geometry-aware 3d generative adversarial networks. In *Proceedings of the IEEE/CVF conference on computer vision and pattern recognition*, 16123–16133.
- Choe, J.; Choy, C.; Park, J.; Kweon, I. S.; and Anandkumar, A. 2023. Spacetime surface regularization for neural dynamic scene reconstruction. In *Proceedings of the IEEE/CVF International Conference on Computer Vision*, 17871–17881.
- Du, Y.; Zhang, Y.; Yu, H.-X.; Tenenbaum, J. B.; and Wu, J. 2021. Neural radiance flow for 4d view synthesis and video processing. In *2021 IEEE/CVF International Conference on Computer Vision (ICCV)*, 14304–14314. IEEE Computer Society.
- Duan, Y.; Wei, F.; Dai, Q.; He, Y.; Chen, W.; and Chen, B. 2024. 4d gaussian splatting: Towards efficient novel view synthesis for dynamic scenes. *arXiv e-prints*, arXiv:2402.00583, 2(3).
- Duisterhof, B. P.; Mandi, Z.; Yao, Y.; Liu, J.-W.; Shou, M. Z.; Song, S.; and Ichnowski, J. 2023. Md-splatting: Learning metric deformation from 4d gaussians in highly deformable scenes. *arXiv preprint arXiv:2312.00583*, 2(3).
- Fang, J.; Yi, T.; Wang, X.; Xie, L.; Zhang, X.; Liu, W.; Nießner, M.; and Tian, Q. 2022. Fast dynamic radiance fields with time-aware neural voxels. In *SIGGRAPH Asia 2022 Conference Papers*, 1–9.
- Fridovich-Keil, S.; Meanti, G.; Warburg, F. R.; Recht, B.; and Kanazawa, A. 2023. K-planes: Explicit radiance fields in space, time, and appearance. In *Proceedings of the IEEE/CVF Conference on Computer Vision and Pattern Recognition*, 12479–12488.
- Gao, C.; Saraf, A.; Kopf, J.; and Huang, J.-B. 2021. Dynamic view synthesis from dynamic monocular video. In *Proceedings of the IEEE/CVF International Conference on Computer Vision*, 5712–5721.
- Huang, Y.-H.; Sun, Y.-T.; Yang, Z.; Lyu, X.; Cao, Y.-P.; and Qi, X. 2024. Sc-gs: Sparse-controlled gaussian splatting for editable dynamic scenes. In *Proceedings of the IEEE/CVF conference on computer vision and pattern recognition*, 4220–4230.
- Kerbl, B.; Kopanas, G.; Leimkühler, T.; and Drettakis, G. 2023. 3D Gaussian splatting for real-time radiance field rendering. *ACM Trans. Graph.*, 42(4): 139–1.
- Kratimenos, A.; Lei, J.; and Daniilidis, K. 2024. Dynmf: Neural motion factorization for real-time dynamic view synthesis with 3d gaussian splatting. In *European Conference on Computer Vision*, 252–269. Springer.
- Kwak, S.; Kim, J.; Jeong, J. Y.; Cheong, W.-S.; Oh, J.; and Kim, M. 2025. MoDec-GS: Global-to-Local Motion Decomposition and Temporal Interval Adjustment for Compact Dynamic 3D Gaussian Splatting. In *Proceedings of the IEEE/CVF Conference on Computer Vision and Pattern Recognition (CVPR)*.
- Li, T.; Slavcheva, M.; et al. 2022. Neural 3d video synthesis from multi-view video. In *Proceedings of the IEEE/CVF conference on computer vision and pattern recognition*, 5521–5531.
- Li, Z.; Chen, Z.; Li, Z.; and Xu, Y. 2024. Spacetime gaussian feature splatting for real-time dynamic view synthesis. In *Proceedings of the IEEE/CVF Conference on Computer Vision and Pattern Recognition*, 8508–8520.
- Liang, Y.; Khan, N.; Li, Z.; Nguyen-Phuoc, T.; Lanman, D.; Tompkin, J.; and Xiao, L. 2023. Gaufré: Gaussian deformation fields for real-time dynamic novel view synthesis. *arXiv preprint arXiv:2312.11458*.
- Liang, Y.; Laidlaw, E.; et al. 2023. Semantic attention flow fields for monocular dynamic scene decomposition. In *Proceedings of the IEEE/CVF International Conference on Computer Vision*, 21797–21806.
- Lin, Y.; Dai, Z.; Zhu, S.; and Yao, Y. 2024. Gaussian-flow: 4d reconstruction with dynamic 3d gaussian particle. In *Proceedings of the IEEE/CVF Conference on Computer Vision and Pattern Recognition*, 21136–21145.
- Liu, Y.-L.; Gao, C.; Meuleman, A.; Tseng, H.-Y.; Saraf, A.; Kim, C.; Chuang, Y.-Y.; Kopf, J.; and Huang, J.-B. 2023. Robust dynamic radiance fields. In *Proceedings of the IEEE/CVF Conference on Computer Vision and Pattern Recognition*, 13–23.
- Lu, Z.; Guo, X.; Hui, L.; Chen, T.; Yang, M.; Tang, X.; Zhu, F.; and Dai, Y. 2024. 3d geometry-aware deformable gaussian splatting for dynamic view synthesis. In *Proceedings of the IEEE/CVF Conference on Computer Vision and Pattern Recognition*, 8900–8910.
- Luiten, J.; Kopanas, G.; Leibe, B.; and Ramanan, D. 2024. Dynamic 3d gaussians: Tracking by persistent dynamic view synthesis. In *2024 International Conference on 3D Vision (3DV)*, 800–809. IEEE.
- Martin-Brualla, R.; Radwan, N.; Sajjadi, M. S.; Barron, J. T.; Dosovitskiy, A.; and Duckworth, D. 2021. Nerf in the wild:

- Neural radiance fields for unconstrained photo collections. In *Proceedings of the IEEE/CVF conference on computer vision and pattern recognition*, 7210–7219.
- Mildenhall, B.; Srinivasan, P. P.; Tancik, M.; Barron, J. T.; Ramamoorthi, R.; and Ng, R. 2021. Nerf: Representing scenes as neural radiance fields for view synthesis. *Communications of the ACM*, 65(1): 99–106.
- Müller, T.; Evans, A.; Schied, C.; and Keller, A. 2022. Instant neural graphics primitives with a multiresolution hash encoding. *ACM transactions on graphics (TOG)*, 41(4): 1–15.
- Park, J.; Bui, M.-Q. V.; Bello, J. L. G.; Moon, J.; Oh, J.; and Kim, M. 2024. SplineGS: Robust Motion-Adaptive Spline for Real-Time Dynamic 3D Gaussians from Monocular Video. *arXiv preprint arXiv:2412.09982*.
- Park, K.; Sinha, U.; Barron, J. T.; Bouaziz, S.; Goldman, D. B.; Seitz, S. M.; and Martin-Brualla, R. 2021a. Nerfies: Deformable neural radiance fields. In *Proceedings of the IEEE/CVF international conference on computer vision*, 5865–5874.
- Park, K.; Sinha, U.; Hedman, P.; Barron, J. T.; Bouaziz, S.; Goldman, D. B.; Martin-Brualla, R.; and Seitz, S. M. 2021b. Hypernerf: A higher-dimensional representation for topologically varying neural radiance fields. *arXiv preprint arXiv:2106.13228*.
- Pumarola, A.; Corona, E.; Pons-Moll, G.; and Moreno-Noguer, F. 2021. D-nerf: Neural radiance fields for dynamic scenes. In *Proceedings of the IEEE/CVF conference on computer vision and pattern recognition*, 10318–10327.
- Shao, R.; Zheng, Z.; Tu, H.; Liu, B.; Zhang, H.; and Liu, Y. 2023. Tensor4d: Efficient neural 4d decomposition for high-fidelity dynamic reconstruction and rendering. In *Proceedings of the IEEE/CVF Conference on Computer Vision and Pattern Recognition*, 16632–16642.
- Tancik, M.; Casser, V.; Yan, X.; Pradhan, S.; Mildenhall, B.; Srinivasan, P. P.; Barron, J. T.; and Kretzschmar, H. 2022. Block-nerf: Scalable large scene neural view synthesis. In *Proceedings of the IEEE/CVF conference on computer vision and pattern recognition*, 8248–8258.
- Tretschk, E.; Tewari, A.; et al. 2021. Non-rigid neural radiance fields: Reconstruction and novel view synthesis of a dynamic scene from monocular video. In *Proceedings of the IEEE/CVF International Conference on Computer Vision*, 12959–12970.
- Wang, C.; MacDonald, L. E.; Jeni, L. A.; and Lucey, S. 2023. Flow supervision for deformable nerf. In *Proceedings of the IEEE/CVF Conference on Computer Vision and Pattern Recognition*, 21128–21137.
- Wang, Z.; Bovik, A. C.; Sheikh, H. R.; and Simoncelli, E. P. 2004. Image quality assessment: from error visibility to structural similarity. *IEEE transactions on image processing*, 13(4): 600–612.
- Wu, G.; Yi, T.; Fang, J.; Xie, L.; Zhang, X.; Wei, W.; Liu, W.; Tian, Q.; and Wang, X. 2024. 4d gaussian splatting for real-time dynamic scene rendering. In *Proceedings of the IEEE/CVF conference on computer vision and pattern recognition*, 20310–20320.
- Xie, T.; Zong, Z.; et al. 2024. Physgaussian: Physics-integrated 3d gaussians for generative dynamics. In *Proceedings of the IEEE/CVF Conference on Computer Vision and Pattern Recognition*, 4389–4398.
- Xu, J.; Fan, Z.; Yang, J.; and Xie, J. 2024. Grid4D: 4D Decomposed Hash Encoding for High-Fidelity Dynamic Gaussian Splatting. *arXiv preprint arXiv:2410.20815*.
- Yang, G.; Vo, M.; et al. 2022. Banmo: Building animatable 3d neural models from many casual videos. In *Proceedings of the IEEE/CVF Conference on Computer Vision and Pattern Recognition*, 2863–2873.
- Yang, Z.; Gao, X.; Zhou, W.; Jiao, S.; Zhang, Y.; and Jin, X. 2024. Deformable 3d gaussians for high-fidelity monocular dynamic scene reconstruction. In *Proceedings of the IEEE/CVF conference on computer vision and pattern recognition*, 20331–20341.
- Yang, Z.; Yang, H.; Pan, Z.; and Zhang, L. 2023. Real-time photorealistic dynamic scene representation and rendering with 4d gaussian splatting. *arXiv preprint arXiv:2310.10642*.
- Yoo, J.-C.; and Han, T. H. 2009. Fast normalized cross-correlation. *Circuits, systems and signal processing*, 28: 819–843.
- Yu, H.; Julin, J.; Milacski, Z. Á.; Niinuma, K.; and Jeni, L. A. 2024. Cogs: Controllable gaussian splatting. In *Proceedings of the IEEE/CVF Conference on Computer Vision and Pattern Recognition*, 21624–21633.
- Zhu, R.; Liang, Y.; Chang, H.; Deng, J.; Lu, J.; Yang, W.; Zhang, T.; and Zhang, Y. 2024. Motiongs: Exploring explicit motion guidance for deformable 3d gaussian splatting. *Advances in Neural Information Processing Systems*, 37: 101790–101817.